View metadata, citation and similar papers at core.ac.uk

brought to you by CORE

provided by University of Queensland eSpace

Molecular Vision 2006; 12:616-25 <http://www.molvis.org/molvis/v12/a68/>
Received 28 February 2005 | Accepted 19 April 2006 | Published 26 May 2006

©2006 Molecular Vision

Nanoparticle tethered antioxidant response element as a biosensor for oxygen induced toxicity in retinal endothelial cells

Tarl Prow,[1] Rhonda Grebe,[1] Carol Merges,[1] Jacob N. Smith,[2] D. Scott McLeod,[1] James F. Leary,[2,3,4] Gerard A. Lutty[1]

[1]The Wilmer Ophthalmological Institute, Department of Ophthalmology, The Johns Hopkins Hospital, Baltimore, MD; Departments of [2]Infectious Diseases and [3]Pathology, University of Texas Medical Branch, Galveston, TX; [4]Basic Medical Sciences and Biomedical Engineering, Purdue University, West Lafayette, IN

Purpose: A novel system, based on biosensor DNA tethered to a nanoparticle, was developed for the treatment of retinopathy of prematurity.
Methods: The construction of a five-layered nanoparticle was visualized with gel electrophoresis. Transcriptionally active PCR products (TAP) containing the biosensor sequence, were bioconjugated to the surface of magnetic nanoparticles yielding biosensor tethered magnetic nanoparticles (MNP). The biosensor was based on an enhanced green fluorescent protein (EGFP) reporter gene driven by an enhanced antioxidant response element (ARE). Image analysis and flow cytometry were used to characterize MNP delivery and biosensor activity.
Results: The MNP penetrated dividing and migrating cells more often than quiescent endothelial cells in a wound-healing in vitro assay. Prussian blue staining demonstrated that more cells have nanoparticle cores than are transfected. When compared to naked TAP alone, MNP transfected more cells in a dose dependent manner. Both the biosensor alone and MNP induce gene expression in the presence of hyperoxia, greater than 1.5 fold over normoxic controls. These data also show that the MNP had a signal to noise ratio of 0.5 greater than the plasmid form of the biosensor as demonstrated by flow cytometry.
Conclusions: This approach has the potential to allow the endothelial cells of the retinal vasculature to prevent or treat themselves after hyperoxic insult, rather than systemic treatment to protect or treat only the retina.

Reactive oxygen species (ROS) are thought to contribute to many retinal microvascular diseases, including diabetes [1-3] and retinopathy of prematurity (ROP) [4,5]. Retinopathy of prematurity was the leading cause of blindness in American infants in the late 1940s [6]. Once hyperoxia was implicated as a causative agent, the exposure of premature infants to hyperoxia was reduced and, subsequently, the incidence of ROP was greatly diminished [7]. Presently, however, the number of blinding ROP cases is increasing again, a result of the larger number of at-risk premature infants surviving [8]. The only proven treatments for ROP being used clinically are retinal ablation by laser or cryotherapy. Ablative therapy causes destruction of the peripheral avascular retina with the intent of destroying the tissue that is the source of angiogenic factor. Although successful at reducing the incidence of blindness associated with threshold ROP in some cases, ablation therapies are associated with reduced visual function [9,10].

The canine model of oxygen-induced retinopathy (OIR) closely resembles human ROP [10], as suggested by Gole [11]. The extent of vaso-obliteration in response to hyperoxia is comparable to human and not limited to central retina like the rodent models. The vasoproliferative response after returning to room air is robust and of long duration like the human and not limited to the short window in which angiogenesis occurs in rodent models. In addition, the neonatal dog eye is comparable in morphology and only slightly smaller in size than premature human, so it can provide a preclinical forum for evaluation of therapeutic reagents. A potential target for ROP therapeutics is hyperoxia-induced oxidative stress.

Oxidative stress levels are communicated through signaling pathways resulting in the induction of antioxidant genes as a protective measure in cells [12-14]. The cell protects itself from oxidative insult through a variety of signaling pathways that converge onto the multitude of promoter sequences found in the genomic DNA. From bacteria to human beings, oxidative stress can be sensed and responded to by a series of proteins including powerful antioxidants and support enzymes. These critical proteins are therapeutic to the cell, in that their presence helps to eliminate oxidative stress. The regulation of these genes can be complex, but recent advances have shed light on some of these pathways. One of these responses is coordinated through a complex signaling network involving the antioxidant response element (ARE) [15,16]. The ARE is composed of a cis-acting enhancer region known as the ARE that is directly controlled by several factors that include the transcription factor Nrf2, a repressor Keap1, and small Maf proteins. This system is endogenously activated through the actions of oxidative stress on the Keap1 protein [17]. This protein normally represses the Nrf2 activator by retaining Nrf2 in the cytoplasm. The activated ARE enhances the expression of any gene downstream of its sequence. The ARE can induce

Correspondence to: Dr. Gerard Lutty, The Wilmer Ophthalmological Institute, 170 Woods Research Building, The Johns Hopkins Hospital, Baltimore, MD, 21287-9115; Phone: (410) 955-6750; FAX: (410) 955-3447; email: galutty@jhmi.edu

a variety of antioxidant and supporting genes (e.g., glutathione s-transferase and NAD(P)H:quinone oxidoreductases) [18,19]. Zhu et al. [20-22] reported the activity of a series of ARE repeats using a EGFP reporter. We adapted this system for use with our nanoparticle-based gene delivery system. This antioxidant response element biosensor approach was chosen because of its potential to control the expression of therapeutic genes for endothelial cells in OIR treatment.

The focus of this study was to develop a nonviral methodology for the delivery of therapeutic genes whose expression would be primarily controlled by the affected cell. This approach helps to alleviate the expression problems associated with the use of promoters; for example, CMV expresses therapeutic or reporter genes at levels far exceeding physiologic levels. Additionally, this approach gives the cell the ability to regulate the therapeutic gene expression in response to the levels of the pathogenic process in real time. Nanoparticles were chosen for these studies, because they have several advantages over more traditional methods, for example viral gene delivery. Viral gene delivery is quite efficient in vitro, but using a virus to deliver genes in vivo is difficult and there can be complications. One of the problems is that the natural viral tropism is altered when a virus is used for gene delivery. Directing a virus to an abnormal host is becoming more and more common as the technology of pseudotyping advances, but this targeting methodology is still in the development stage. This is done by changing the exposed proteins on the viral surface. Another problem in this process is the immunoreactivity of the virus, which is currently being minimized through the development of chimeric viruses [23]. The transduction efficiency for viral-based gene delivery vectors is usually determined by fluorescence or clonal selection. In fact, most if not all of the viral vectors are not replication competent, thus requiring a packaging cell line to be produced. After production, the virus then needs to be purified from the contaminants in the cell media [24]. If done incorrectly, the immunogenicity can be greatly enhanced. In vivo transfection varies greatly depending on the virus, genetic elements used, and the tissue treated [24].

On the other hand, magnetic nanoparticles, like the ones used in this manuscript, do not appear to illicit an immune response, even when targeted to immune cells [25]. These and other nanoparticles can be synthesized to carry any number of molecules, including proteins, DNA, lipids and, organic and

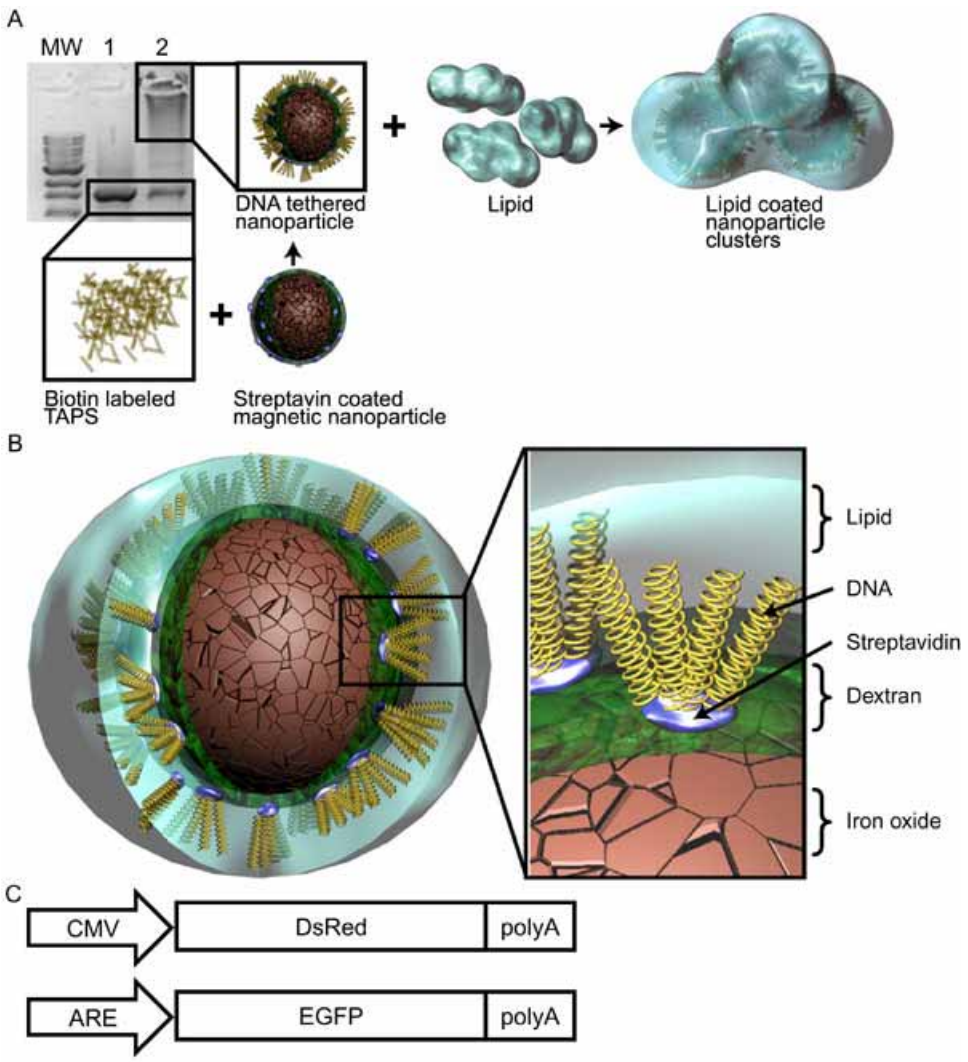

Figure 1. Construction and anatomy of magnetic nanoparticles. **A**: Conjugation of biotin-labeled transcriptionally active PCR products (TAP) DNA to streptavidin-coated magnetic nanoparticles (MNP). A 0.8% agarose gel stained with ethidium bromide was used to visualize DNA and DNA tethered nanoparticles. The leftmost lane are molecular weight markers, from 1 to 10 kb (MW). Lane 1 contains only 5' biotin-tagged TAP DNA (Black rectangular outline). Lane 2 is a solution containing DNA from Lane 1 combined with streptavidin-coated magnetic nanoparticles. The black rectangular outline in Lane 2 highlights 5' TAP tethered magnetic nanoparticles. **A**: Schematic of the construction of the MNP. **B**: The layered anatomy of a lipid coated DNA tethered nanoparticle. **C**: Schematics of the two DNA constructs used to assess transfection and ARE activity.

inorganic substances [26]. Therefore, the flexibility of the targeting system of a nanoparticle is much greater than that of a naturally produced virus. Some other advantages of nanotechnology in this arena are low immunogenicity, multifunctional components on individual layers (Figure 1), inability to reproduce, and biodegradability. In the near future we will probably design synthetic viruses that carry out simple targeted gene delivery, but the true benefit from nano-scaled synthesis will be realized when we make multifunctional nano-scaled tools to address complex diseases. This study describes, in detail, the construction and characterization of TAP-tethered magnetic nanoparticles (MNP) for the delivery of genes in vitro. These data suggest that MNP most efficiently transfect migrating and dividing retinal endothelial cells. Finally, we show that canine retinal endothelial cells induce a nanoparticle delivered biosensor activity (ARE) in response to hyperoxia.

METHODS

Primary culture of adult dog retinal endothelial cells (ADREC): Primary cell lines of ADRECs were established as reported in the companion manuscript and by Lutty et al. [27]. Adult beagles were euthanized by an intraperitoneal overdose of pentobarbital sodium. Animals were treated in accordance with the ARVO Statement for the Use of Animals in Ophthalmic and Vision Research. The eyes were enucleated and then soaked in cold Betadine for 15 min. The retina was dissected, washed thoroughly, and homogenized in PBS with a Dounce homogenizer. The homogenate was filtered with a 105 μm Nitex nylon mesh in a porcelain funnel under a gentle vacuum. The filtrate was then passed through an 58 μm Nitex mesh. The vessel retentate was digested in 0.375% collagenase and 0.25% bovine serum albumin in PBS for 45-60 min at 37 °C. The digestion was then stopped by the addition of DMEM/F12 media supplemented with 10% fetal bovine serum, 1% Penicillin/Streptomycin/Fungizone (Gibco, Inc., Rockville, MD). The cells were then incubated at 37 °C in 5% CO_2 for 24 h in a T-25 flask. After 24 h, the unattached cells and debris were washed away and the remaining cells were given fresh media. All studies were done with cells less than passage 10. Cells were 100% positive for vWF and uptake of acetylated low density lipoprotein.

Adult dog retinal endothelial cells wound healing assay: A wound healing assay described by Selden et al. [28] was used for generating quiescent, dividing, and migrating ADRECs in culture [27]. Cells were first grown to confluence in 24 well plates and then wounds were made by scraping laterally across the dish surface with a sterile razor blade. The edge of the razor scores the plastic dish slightly at the beginning of the stroke and the razor removes all cells in its path. The wells are rinsed once with PBS, pH 7, to remove the non-adherent cells and then fresh media added. The cells were then incubated as above for 48 h prior to treatment. After treatment with 0, 5, 10, or 20 μl of MNP, the morphology of the cells was examined and quantified. Quiescent cells are the cells that were still present in the monolayer after scraping (i.e., were located behind the scrape line). The dividing and migrating cells are the cells that have progressed into the region where cells were removed. Migrating cells were elongated and displayed processes, whereas dividing cells were rounded and raised. Migrating cells are mostly in advance of dividing cells in the wound repair process [28]. Three fields were photographed per well and a total of three wells were examined per group. An example of a field is shown in Figure 2.

Generation of TAP: PCR amplification was used to create biotin-labeled DNA fragments. For initial studies, either the 5' or the 3' oligonucleotide was made with a single biotin tag. The sequences were based on the pDsRed-C1 (BD Clontech, Inc., Mountain View, CA) and pARE templates: forward 5'-TAG TTA TTA ATA GTA ATC-3', reverse 5'-TAC ATT GAT GAG TTT GGA-3' (Integrated DNA Technologies, Inc., Coralville, IA). The pARE template was generously donated by William Fahl (University of Wisconsin, Madison, WI) and Ming Zhu (Arizona Cancer Center, Tuscon, AZ). Later studies used only oligonucleotides labeled with a 5' biotin. These oligonucleotides were then used as PCR primers. For ARE studies, a typical reaction would include: 25 μl Red Taq, (5 units, Sigma Chemicals, Inc., St. Louis, MO), 1 μl 5' biotinylated primer, 1 μl 3' primer, 1 μl template, 5 μl PCR buffer (containing 100 mM Tris-HCl, pH 8.3, 500 mM KCl, 11 mM $MgCl_2$ and 0.1% gelatin), and 17 μl water. The oligonucleotides were at 200 pM and the template at 50 ng/μl. A typical reaction for DNA tethering to magnetic nanoparticles would include about 25 of these reactions. Typical PCR cycles would include 35 cycles of denaturing at 94 °C for 30 s, annealing at 65 °C for 30 s and extension for 2 min at 72 °C. Normally, 96 reactions were carried out for each experiment.

MNP construction: Biotin-labeled TAP were tethered to streptavidin-coated magnetic nanoparticles (Miltenyi Biotech, Inc., Auburn, CA; Figure 1). The magnetic nanoparticles were incubated with the biotin-labeled PCR fragments at about 30 ng of 1.5 kb TAP per 1 μl of nanoparticles. The mixture was allowed to incubate at room temperature for 30 min. During that time, the magnetic column (Miltenyi Biotech, Inc.) was prepared by washing once with 100 μl of the included nucleic acid buffer and three times with 100 μl Optimem (Gibco, Inc.). Once washed, the column was loaded with the DNA nanoparticle mixture. The column was then washed three times with 100 μl Optimem. The nanoparticles were eluted by removing the column from the magnet and adding 100 μl of Optimem. The MNP were then coated with lipid (Lipofectamine 2000, Invitrogen, Inc., Carlsbad, CA). The lipid coating procedure used the amount of DNA to determine the quantity of lipid added. For example, when 4 μg of TAP were tethered to nanoparticles, the eluted nanoparticles were diluted in 250 μl of Optimem and incubated for 5 min at room temperature. While incubating, 10 μl of lipid was added to another 250 μl of Optimem and incubated for the remaining time. After 5 min, the two tubes were mixed gently and combined. This mixture was allowed to stand for 20 min before being added to the cell culture (i.e., one well of a six well plate).

MNP transfection: The transfection solution containing complete MNP in Optimem, was incubated with the cells at 37 °C overnight. For 6 well plates, 500 μl of MNP solution

(with 4 μg of DNA) was added to 2 ml of normal media in a single well. After the overnight incubation, the cells were washed once with PBS and then incubated with complete media for the remainder of the experiment. This procedure was carried out for all experiments except for those involving hyperoxia. For the cells that were exposed to MNP in hyperoxia experiments, we used a slightly modified transfection protocol to yield higher transfection efficiencies while maintaining viability. For this experiment, the media was removed from a growing culture in a single 6 well plate and 250 μl the MNP suspension containing 4 μg of DNA was added to a single well of a 6 well plate. The cells were then incubated in cell culture conditions (37 °C in 5% CO_2) for 2 h. The plates were rocked every 10 min to maintain equal dispersion of the MNP. After 2 h the cultures were washed once with PBS and fed normal culture medium.

Agarose gel electrophoresis: Agarose gel (0.8%, Cambrex Bio Science Rockland, Inc., Rockland, ME) electrophoresis

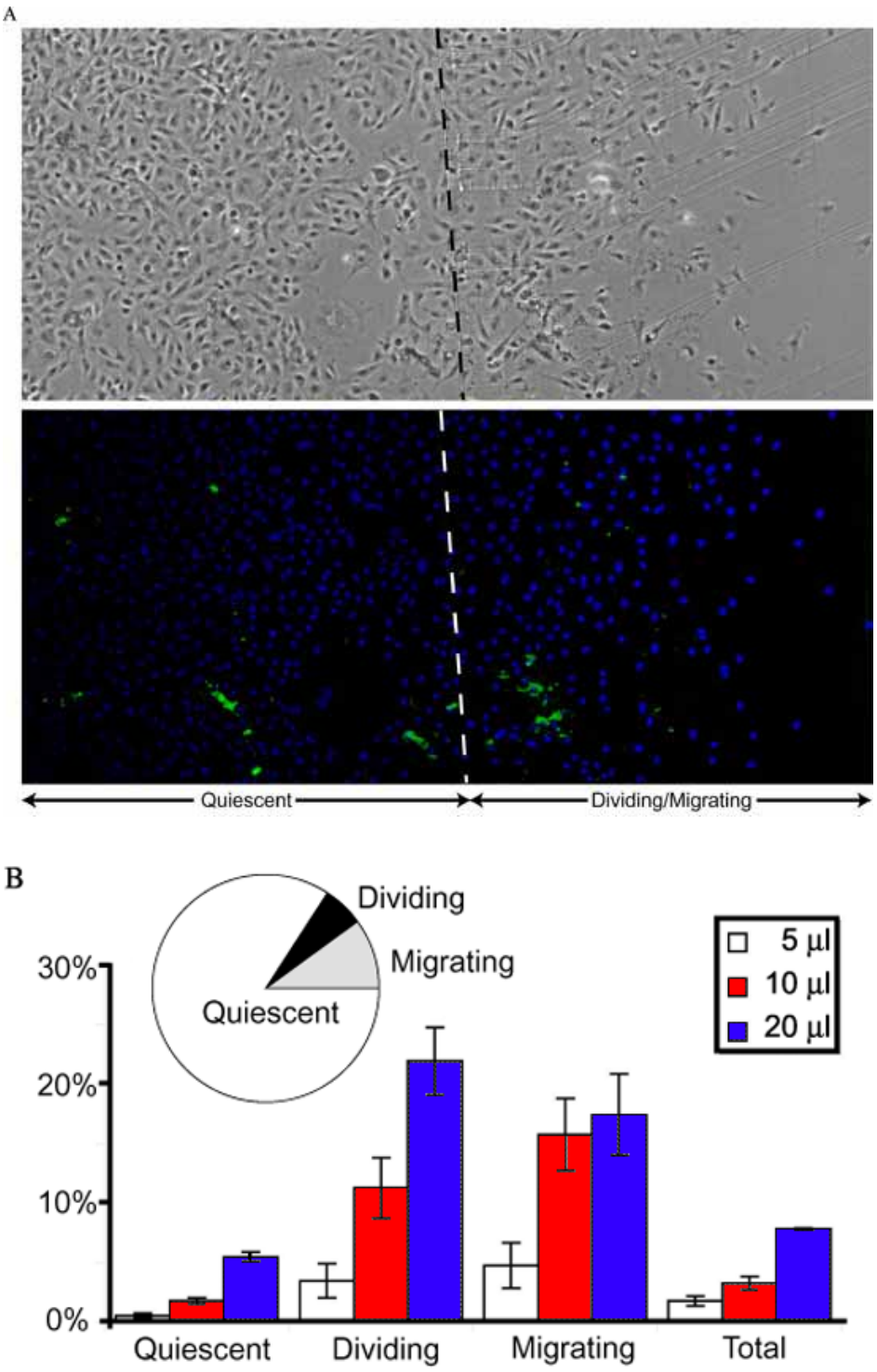

Figure 2. Characterization of magnetic nanoparticle penetration. Twenty four h after nanoparticle treatment the cells were developed for alkaline phosphatase activity (pseudocolored green). **A**: Phase contrast (top) and pseudocolored (bottom) micrographs of a typical field containing quiescent, dividing, and migrating ADRECs. Nuclei were counterstained with DAPI (blue, bottom panel). The scrape line is visible at the junction between the quiescent and dividing/migrating cells (dashed line). This field was part of a well (from a 24 well plate) that was treated with 20 μl of alkaline phosphatase protein coated nanoparticles. **B**: Graphs of data from image analysis of nanoparticle-treated cells. The cell morphology (quiescent, dividers, and migrators) was used as a basis for determining nanoparticle targeting trends. The mean percent and standard deviation of positive cells was calculated from an n=3. At least 2000 cells were analyzed from each group. The cells were treated with one of four volumes (μl) of a single preparation of nanoparticles (0, 5, 10, and 20 μl) which permitted the dose response to be determined in various cell morphology groups. The inset is a pie chart showing the proportions of the three cell types in the samples analyzed.

was used to visualize DNA and MNP. Electrophoresis was carried out at 100 V for a minimum of 20 min. The resulting gel was stained with 5 μg/ml ethidium bromide for 10 min and then de-stained in deionized water for 10 min. Gels were visualized and photographed on a UV light box with a Nikon CoolPix 990 digital camera (Nikon, Inc. Melville, NY). For naked DNA, 1 μl of DNA or PCR product was mixed with 5 μl of 1X loading buffer (New England Biolabs, Inc., Beverly, MA) and then loaded onto the gel. For MNP, 5 μl of the MNP mixture was mixed with 1 μl of 5X loading buffer and then loaded onto the gel.

Fluorescent microscopy and image analysis: All fluorescent microscopy was done on a Nikon Eclipse TE2000-U (Nikon, Inc., Melville, NY). The photomicrographs were taken with a Spot RT SE camera from Diagnostic Instruments, Inc., Sterling Heights, MI. All photomicrographs were taken with the SPOT Advanced software version 3.5.6 (Diagnostic Instruments, Inc.). The cells were fixed in 2% paraformaldehyde in TBS, pH 7.4, for 10 min and then washed three times with TBS prior to being photographed. Phase contrast photomicrographs were taken with an exposure time of 100 ms and at a gain of 1. Fluorescent image photography was tailored to the fluorochrome of interest. Photographs of DsRed or EGFP containing cells were taken with an exposure time of 1.5 s and at a gain of 4. This was determined by limiting the exposure time and gain to levels below saturation in positive control samples.

DAPI or Hoechst 33342 stained cells were photographed with an exposure time of 100 ms and at a gain of 1. All images were saved as full resolution, RGB tiffs. Image analysis was done with NIH image. For nuclei counts, the tiff image was imported into NIH image and the threshold function was applied at a cutoff value of 50. Then, the number of nuclei were counted using the analyze particles function with a minimum size of 100. The resulting data was then imported into Excel (Microsoft, Inc., Redmond, WA) and analyzed. All schematics were done in Photoshop and Illustrator (Adobe Systems, Inc., San Jose, CA).

Alkaline phosphatase staining: For alkaline phosphatase staining, the cells were first fixed in 2% paraformaldehyde in tris-buffered saline pH 7 (TBS) for 10 min at room temperature. Then, the cells were permeabilized with 0.25% triton X-100 in TBS for 10 min at room temperature. Endogenous alkaline phosphatase activity was inhibited with the addition of 10 mM levamisole to the development solution. The MNP delivered alkaline phosphatase (New England Biolabs, Inc.) activity was detected with the BCIP/NBT alkaline phosphatase substrate kit from Vector Labs, Inc. Burlingame, CA. The development solution contained 2 drops of the Vector Labs reagents A, B, and C in 5 ml of 100 mM Tris-HCl, pH 9.5. This solution was then filtered through a 0.22 μm syringe filter prior to use. The cells were washed three times with 100 mM Tris-HCl, pH 9.5, prior to development. The alkaline phosphatase activity was developed for 30 min at room temperature in the dark. After development, the cells were washed and stored in TBS at 4 °C. Positive cells contained dark purple or blue coloration, whereas negative cells had no coloration.

Prussian blue staining: Prussian blue staining was used to detect cells that contained magnetic nanoparticles [29]. This does not imply that the cells contain complete MNP, just the iron oxide core of the nanoparticle. The cells were fixed and permeabilized as described above and counterstained with 1 μg/ml Hoechst 33342 for 15 min, prior to Prussian Blue staining. A staining solution containing equal parts 20% hydrochloric acid and 10% potassium ferrocyanide was applied to cells for 10 to 20 min at room temperature. Positive reactions generally occurred promptly and looked like blue spots within the cell. These blue spots are the result of the ferric iron in the nanoparticles combined with the potassium ferrocyanide to form ferric-ferrocyanide, which has a bright blue color. Analysis was done by first photographing a field under light and UV fluorescence, followed by NIH image analysis of the fluorescence images and hand counting the Prussian Blue positive cells.

Immunocytochemistry: Cells were transfected with nothing, pEGFP-N1, TAP-EGFP (containing CMV-EGFP-N1-pA), and MNP-EGFP (containing TAP-EGFP) as described above. After 24 h, the cells were rinsed with TBS three times and fixed with 2% paraformaldehyde for 10 min at room temperature. The cells were then washed three times with TBS and permeabilized with 0.1% Triton-X 100 for 10 min at room temperature. The cells were then washed three times with TBS prior to using an avidin/biotin blocking kit containing Avidin D and biotin to block free biotin and any available streptavidin binding sites on the MNP (Vector Laboratories, Burlingame, CA). After blocking, the cells were washed with TBS and incubated with the primary antibody, goat anti-GFP at 1:10,000 (Abcam, Cambridge, UK) for 2 h at room temperature. After primary labeling and washing, the cells were incubated with the secondary antibody at 1:4000, biotinylated mouse anti-goat IgG (Jackson ImmunoResearch, West Grove, PA) for 30 min at room temperature. The cells were then washed with TBS and incubated with streptavidin-conjugated alkaline phosphatase at 1:2000 (KPL, Gaithersburg, MD) for 30 min at room temperature. The cells were washed and alkaline phosphatase activity developed with the BCIP/NBT substrate kit (Vector Labs) supplemented with 2 mg/5 ml Levamisole (Sigma Chemicals, Inc.) for 10 min at room temperature. The cells were then washed with TBS and distilled water prior to analysis. The positive and negative cells were then counted on a light microscope with a 40x objective. Five fields in three wells were counted per group and the Student's t-test used to determine statistical significance.

Flow cytometry: After exposing the cells to either normoxia or hyperoxia for 3 days, the cells were washed once with PBS and stained with 1 μg/ml Hoechst 33342 for 10 min. The cells were then photographed. After photo-documentation, the cells were incubated with 0.1% trypsin for 5 min. The trypsin was then inhibited by the addition of 5 ml complete media. The cells were then pipetted into a 15 ml conical tube (Corning, Inc., Corning, NY) and centrifuged at 2000 RPM in a Beckman TJ-6 centrifuge with a Beckman TH-4 rotor for 10 min. The cells were then washed three times with PBS prior to fixation in cold 70% ethanol in PBS overnight.

The following day the cells were analyzed on a BD FACScan using channel FL1 for EGFP fluorescence. The FL1 gain was set at 350. The resulting data were analyzed on a PC using WinMDI (The Scripps Research Institute, La Jolla, CA).

RESULTS

Construction and anatomy of MNP: In early studies, reporter genes were used to characterize the nanoparticles and their ability to transfect cells (See companion manuscript). Some early studies substituted biotin-labeled alkaline phosphatase as a reporter for biotin-labeled TAP in order to determine the number and type of cells that contained complete MNP. Figure 1 is a schematic of the MNP construction (Figure 1A), depictions of multilayered nanoparticle anatomy (Figure 1B), and the DNA constructs used in these studies (Figure 1C). Both 5' (Figure 1A) and 3' labeled TAP, with respect to the coding direction, were used for constructing MNP. In the companion manuscript, we determined that there were no differences between the labeling strategies, as far as construction of the MNP was concerned. The 5' biotin tethered TAP showed slightly better reporter gene expression than 3' tethered TAP and, therefore, were used in the following studies. Non biotin-labeled TAP were used as negative control for MNP formation, and as expected did not bind to the magnetic nanoparticles.

Characterization of MNP transfection: Observations from pilot experiments using MNP and cells at different plating densities suggested that transfection efficiency was greater in dividing cells, with respect to quiescent cells. This hypothesis was born out in a study that examined the morphology of cells containing alkaline phosphatase-coated magnetic nanoparticles (Figure 2A,B). A wound healing assay was used to generate quiescent, dividing, and migrating cells from a confluent monolayer by scraping and allowing the cells to regrow [27,28]. The junction between the quiescent and dividing/migrating cells was apparent from the scrape mark and cell migration preceded proliferation in distance from the wound edge (Figure 2A) [28]. After 48 h of regrowth, the cells were treated with alkaline phosphatase coated nanoparticles. After 24 h, the cells were analyzed for alkaline phosphatase activity (pseudocolored green in Figure 2A, lower micrograph). In this example, 29 of 539 quiescent, 17 of 90 dividing, and 16 of 38 migrating cells were positive for complete nanoparticles. These data describe nanoparticle penetration within specific groups, including quiescent, dividing, and migrating cells. A dose dependent preference for dividing/migrating cells was observed, when compared to quiescent cells (Figure 2B). The stock biotin-labeled alkaline phosphatase solution was used at the highest dose (20 µl in 1 ml of media) as a negative control and no positive cells were found in this group. The pie chart inset shows the average proportion of each cell morphologic type examined. Even though the quiescent cells outnumbered the dividing/migrating cells 3 to 1, there were a larger proportion of dividing/migrating cells positive with nanoparticles than quiescent cells.

Figure 3 is a breakdown of penetration and transfection of three different stages of MNP construction in either quiescent or dividing/migrating cells. In contrast to Figure 2, Figure 3 examines the effect of nanoparticle layers on transfection in quiescent and migrating/dividing cells with respect to the entire population of cells. The same scrape assay described above was used to test the hypothesis that the assembly of layered nanoparticles yields both complete and incomplete nanoparticles. This technique is important because it is the first to examine the complex effects of nanoparticle construction on biological functionality. The graph represents the percentage of cells positive for either the iron core, complete nanoparticle (core, tethered protein, and lipid coating), or transfection (expression of a reporter gene tethered to the nanoparticle), all normalized to the total number of core positive cells. Below the bar graph in Figure 3 there are representative photomicrographs of each group. Each of the groups were coated with lipid as described above. All MNP have iron cores, so the cells with MNP could be detected with Prussian Blue staining. This was interpreted as the total number of nanoparticles present (Core). The enzymatic activity of alkaline phosphatase tethered nanoparticles identified cells containing complete nanoparticles (Complete). The supposition that any cell with alkaline phosphatase activity have complete nanoparticles can be made because endogenous alkaline phosphatase activity was inhibited with levamisole and no cells treated with alkaline phosphatase alone had any detectible activity (data not shown). DsRed expression from MNP was used to determine successfully transfected cells (Transfection). All of the data points shown in Figure 3 were derived from a single dose of nanoparticles (20 µl per well). A minimal dose of nanoparticles was used in an attempt to get as close to one nanoparticle per cell dose as possible, so that a clear relationship between the groups could be established. Results indicate that there is a decline in the number of positive cells, after the addition of the first layer. The same trend holds true regardless of cell morphology, although the loss of efficiency is more pronounced in the dividing/migrating cells.

Immunocytochemistry for EGFP was used as a very sensitive way to determine the number of MNP transfected cells versus plasmid and TAP transfected cells. The results of these experiments showed very similar results and relationships to those that have used flow cytometry to evaluate transfection efficiency. The immunocytochemical method has several benefits, including the ability to use enzymatic activity to yield a sensitive and permanent record. Our results showed that the non-transfected cells had little background, while the EGFP positive cells were clearly and very darkly stained. Cells transfected with 400 ng of pEGFP-N1 were 42% positive, while the TAP transfected cells had 70% fewer positive cells. The MNP transfected group showed 27% transfection, which was similar to the results from previous experiments and about twice the level of the TAP group.

Effect of hyperoxia on reporter gene expression and biosensor activity in ADRECs: Flow cytometric analysis of ARE-driven EGFP fluorescence was conducted on ADRECs pooled from 3 identical experiments. Each group was exposed to no DNA, plasmid DNA, or MNP 24 h after plating. These cells were subsequently exposed to normoxia or hyperoxia for 3

days. All cells, including non-transfected, controls (Negative) were incubated in normoxia or hyperoxia for 3 days and then analyzed for EGFP expression with flow cytometry. The negative control-derived data gave a background level of fluorescence and served to help determine the cutoff for EGFP positive cells (set at about 5% of the hyperoxic negative group, Figure 4). The control cell data appeared to have slightly increased fluorescence despite not being exposed to EGFP. This is most likely due to increasing autofluorescence in stressed and dying cells. The MNP-treated cells in hyperoxic conditions showed an obvious increase in the number of EGFP positive cells when compared to the normoxic controls (Figure 4). The level of biosensor activation in normoxic cells treated with MNP (false positive) was about 9% lower than that found in plasmid control cells, 6.28% and 15.22%, respectively. In hyperoxia, the percentage of GFP positive cells rose to 19.84% in MNP treated cells and 40.27% in plasmid treated cells. These data indicate that the MNP is sensitive to hyperoxia (Figure 4). The plasmid DNA-treated cells had higher false positive and true positive results. The fold increase of GFP positive cells in hyperoxia, however, was greater for MNP-treated cells than plasmid-treated cells at 3.16 and 2.65, respectively. Overall, these data show that the MNP tethered biosensor was activated in hyperoxia.

DISCUSSION

Construction and anatomy of MNP: The construction of the MNP was fairly straightforward, when compared to some other

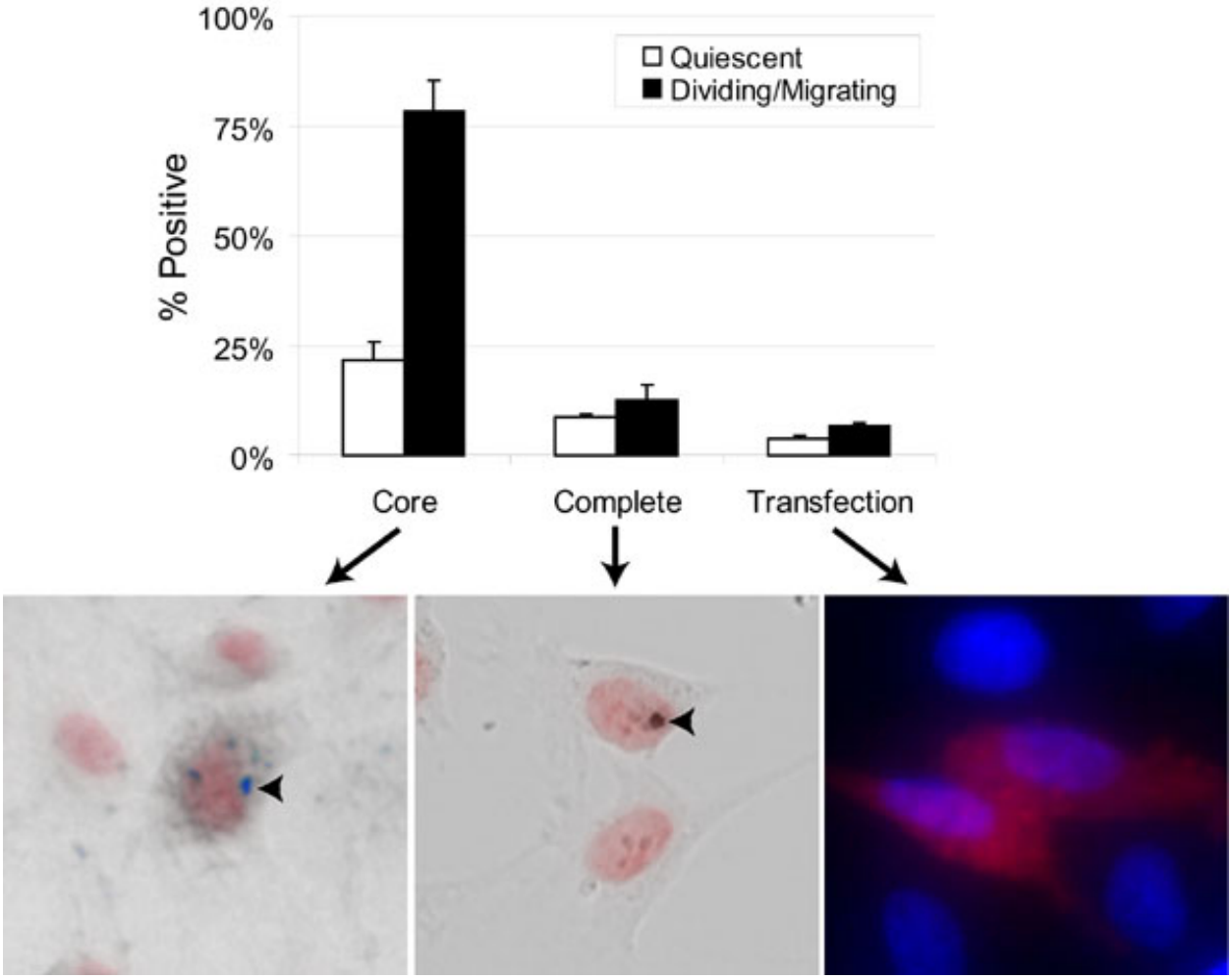

Figure 3. The presence of magnetic nanoparticle components in transfected cells. These data represent a breakdown of the magnetic nanoparticles (MNP) components in either quiescent or dividing/migrating cells. This data set was generated by exposing scraped ADRECs to MNP, which included lipid coated nanoparticles tethered to DsRed DNA (Transfection) or lipid coated nanoparticles tethered to alkaline phosphatase protein (Complete). The same cells used for the Transfection data were later evaluated for the Core data with Prussian blue staining. Prussian blue staining (bottom left, arrow head) for iron was used to quantify the number of cells containing nanoparticles (Core) in the MNP treated cells. The APase activity (bottom center, arrow head) was used as a surrogate for determining the number of cells with complete nanoparticles (Complete). Cells positive for DsRed were quantified to assess the number of successfully transfected cells (Transfection, bottom right photomicrograph, where DsRed is red and Hoechst 33342 counterstain is blue). The cells were treated with a minimal dose of nanoparticles (10 µl per well of a 6 well plate, n=3) and were stained 24 h after nanoparticle treatment. Values are the average of three measurements; error bars represent the standard error of the mean.

gene delivery methods. As expected, the biotin-labeled ARE biosensor did not effect the construction of the MNP. Studies were designed to determine whether the nanoparticles transfected dividing/migrating more often a quiescent cells. These data suggest a preference for MNP transfection in dividing and migrating cells in vitro, which gives valuable insight into their use in vivo. This suggests that the restructuring of the cytoskeleton and cytoplasmic membrane that accompanies division and migration may allow more nanoparticles to gain entry to the cell. These structural changes could be a key to enabling the nanoparticles to penetrate cells in vivo. The dividing/migrating cells may also be more metabolically active and, therefore, have increased pinocytosis compared to quiescent cells. Whatever the mechanism, these data guided us to

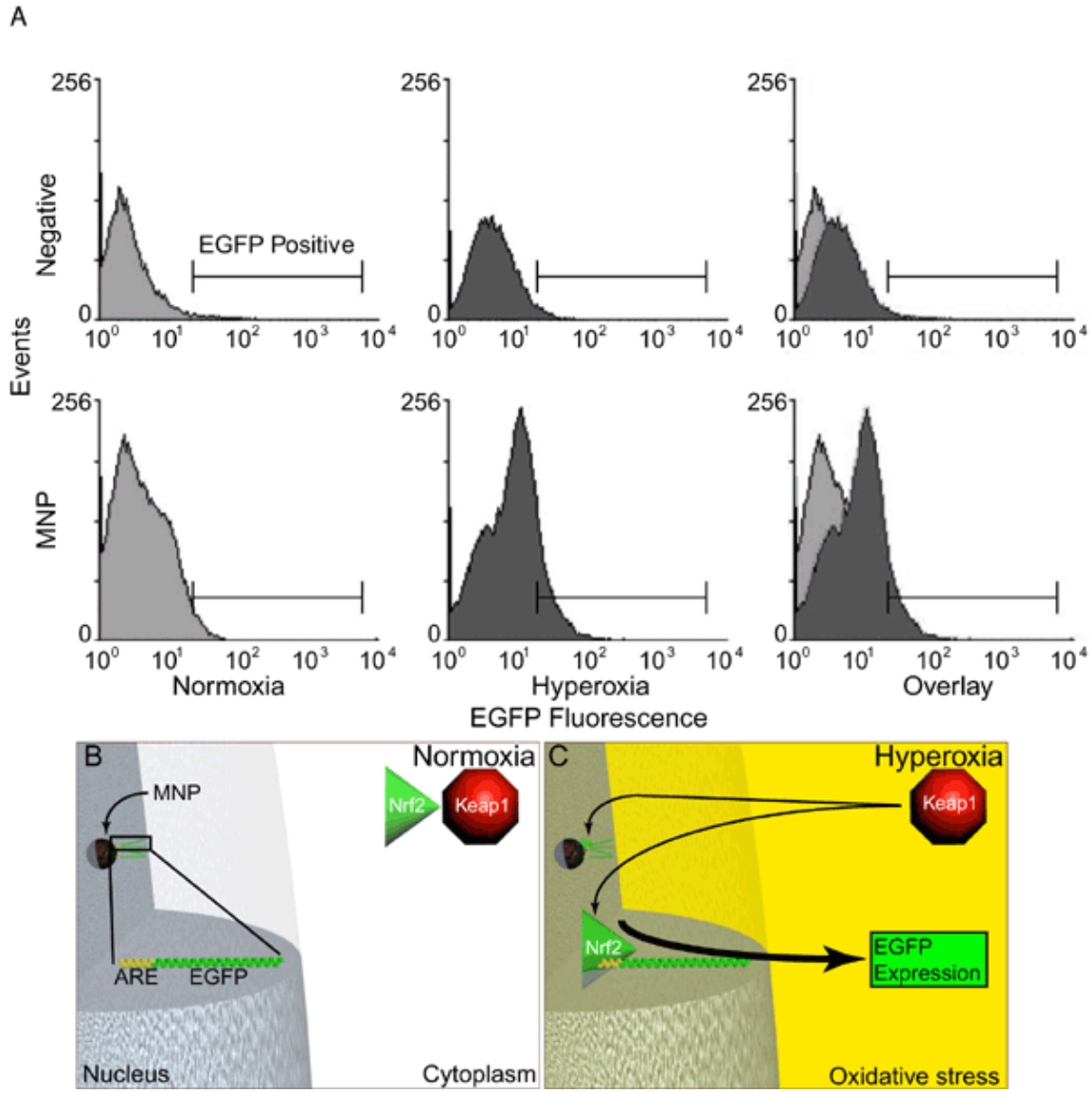

Figure 4. Activity of MNP tethered biosensor in hyperoxia and overview of this process. These flow cytometric data confirm that the cell induces the ARE on the MNP in response to hyperoxic insult, thereby resulting in the increased expression of the ARE driven EGFP reporter. This experiment illustrates the use of a functional biosensor tethered to a MNP that can detect and report a pathological state. **A**: Flow cytometric analysis of biosensor activity. These histograms are from cells exposed to normoxic or hyperoxic conditions, either with or without the biosensor. The right column contains composite images derived from both the normoxic and hyperoxic histograms. The transfection groups are a negative control (Negative, no DNA) and MNP-ARE-EGFP are shown in two rows. The y-axis represents events and the X-axis is GFP fluorescence. The bar indicates the GFP positive region used to calculate the percentage of GFP positive cells. **B**,**C**: An overview of the biosensor tethered nanoparticle in normoxic (**B**) and hyperoxic (**C**) conditions. Under normal conditions, the ARE repressor protein Keap1 (red octagon) prevents the ARE activator Nrf2 (green triangle) from leaving the cytoplasm (**B**). The nanoparticle tethered biosensor (MNP) is localized in the nucleus and consists of the ARE followed by a EGFP reporter gene (ARE EGFP). When exposed to hyperoxia (**C**), the cell experiences oxidative stress. This oxidative insult (yellow) initiates ARE activation by Nrf2 localization in the nucleus, binds to the ARE (thin arrow), and initiates EGFP expression (thick arrow; **C**).

use proliferating cells in order to maximize transfection of the MNP.

To better understand the limits of this technology we examined two levels of MNP construction to cell transfection in a mixed culture of quiescent and dividing/migrating cells. These data demonstrate for the first time the effects of multiple layers on magnetic nanoparticle entry into the cell. We are the first to quantify how many cells have nanoparticles, how many of those cells carry complete nanoparticles, and finally the number of cells that are successfully transfected. These data show that the addition of up to three layers (dextran, streptavidin, and TAP) decreases the number of positive cells from 6 to 1% and only half of those cells that contained complete nanoparticles expressed the transfected reporter gene (accompanying manuscript and Figure 3). These experiments suggest that the addition of each layer could decrease the transfection efficiency by 50% and this number is halved again if the particle requires nuclear localization, which is necessary for transfection. This dramatic stepwise decrease in activity with the addition of layers makes assembly and purification paramount to success with these synthetic, nonviral agents for gene delivery. This information is important because one of the major benefits of using this technology is the ability to add multiple layers, with each having different functions. However, we can use the ability to have multiple layers to add peptides which enhance uptake, nuclear translocation, and transfection efficiency in the future.

Effect of ADREC exposure to hyperoxia on reporter gene expression and biosensor activity: One of the first steps toward developing this strategy was determining if protein expression from MNP was altered by hyperoxia. The ARE was first tested as a plasmid and was found to be induced in cells exposed to hyperoxia. This suggests that the cells are experiencing oxidative stress and are responding by inducing the expression of cellular antioxidants through the ARE pathway. Finally, the biosensor was found to be quite functional when delivered by a MNP. There were also low levels of biosensor activity in normoxic cells. This may indicate a basal level of ARE induction normally found in ADRECs.

Collectively, these data show the detailed construction and characterization of the first biosensor-tethered nanoparticle for autoregulation of a therapeutic gene. Gel electrophoresis confirmed the construction of ARE-tethered magnetic nanoparticles. Dividing and migrating cells were much more likely to be transfected by MNP than quiescent cells. This suggests that this approach will be helpful in treating ROP since migrating cells are organizing to form the retinal vasculature at the time of hyperoxic insult. Transmission electron microscopy images showed most MNP to have perinuclear localization (unpublished results). These images also confirmed that there are differences in core size and the thickness of the layers. Together these data strongly suggest that MNP construction was not 100% efficient. Even so, ARE-tethered MNP were capable of inducing ARE-driven reporter gene expression primarily in the presence of hyperoxia (Figure 4).

These data show that it is possible to deliver a functional biosensor tethered to a nanoparticle. Furthermore, the multilayered nanoparticle system has the advantage of increasing functionality with additional layers. The next step for this promising technology is the addition of therapeutic genes and further optimization for improved transfection prior to moving into an in vivo ROP model. The ARE is quite appropriate for controlling a therapeutic gene, since gene expression was low when the stimulus was not present. Using this system of therapeutic protein delivery has several benefits, when compared to drug or protein delivery. One of the primary advantages of this system is that the therapeutic agent, in this case a protein, can be manufactured by the cell in need. This could help to greatly reduce the need to repeatedly treat the individual. Another benefit of using the ARE is the ability of the individual cell to titer its own drug concentration, thereby treating only the cells that need the therapeutics. The basal expression patterns may be a problem if therapeutic gene expression needs to be kept at a minimum. The problem of high levels of uninduced expression can be ameliorated by modifying the promoter construct to match the optimal dosing strategy. Using this system to treat ROP is valid because many of the cells in the eye are dividing and migrating during this stage of development. This system could then be used to prevent a critical stage of ROP, vaso-obliteration. The data shown herein suggests that this biosensor is capable of being activated upon exposure to hyperoxia. Once activated, the biosensor could be used to drive a multitude of therapeutic genes, including those that minimize the cell death associated with vaso-obliteration and this expression will occur only in cells confronted with oxidative stress. This system also allows one to noninvasively monitor therapeutic gene expression via a fluorescent reporter. The perfect reporter would be one that has no toxicity and absorbs and emits in the far red, to escape the problems associated with autofluorescence. One candidate gene might be the current generation of DsRed monomers [30]. We are currently investigating several candidate genes for this task including antioxidants, DNA repair enzymes, and antiangiogenics (for example pigment epithelium derived factor).

ACKNOWLEDGEMENTS

This work was supported by the Biomolecular, Physics and Chemistry Program under NASA grant NAS2-02059 (JL), National Eye Institute grant R03EY013744 (GL), R01EY09357 (GL), EY01765 (Wilmer), and the Johns Hopkins Hematology Training grant T32HL007525 (TP).

REFERENCES

1. Taniyama Y, Griendling KK. Reactive oxygen species in the vasculature: molecular and cellular mechanisms. Hypertension 2003; 42:1075-81.
2. Yorek MA. The role of oxidative stress in diabetic vascular and neural disease. Free Radic Res 2003; 37:471-80.
3. Obrosova IG, Minchenko AG, Frank RN, Seigel GM, Zsengeller Z, Pacher P, Stevens MJ, Szabo C. Poly(ADP-ribose) polymerase inhibitors counteract diabetes- and hypoxia-induced retinal vascular endothelial growth factor overexpression. Int J Mol Med 2004; 14:55-64.
4. Beauchamp MH, Marrache AM, Hou X, Gobeil F Jr, Bernier SG, Lachapelle P, Abran D, Quiniou C, Brault S, Peri KG, Roberts J

2nd, Almazan G, Varma DR, Chemtob S. Platelet-activating factor in vasoobliteration of oxygen-induced retinopathy. Invest Ophthalmol Vis Sci 2002; 43:3327-37.
5. Papp A, Nemeth I, Karg E, Papp E. Glutathione status in retinopathy of prematurity. Free Radic Biol Med 1999; 27:738-43.
6. Payne JW, Patz A. Current status of retrolental fibroplasia. The retinopathy of prematurity. Ann Clin Res 1979; 11:205-21.
7. Patz A. The role of oxygen in retrolental fibroplasia. Trans Am Ophthalmol Soc 1968; 66:940-85.
8. Phelps DL. Retinopathy of prematurity: an estimate of vision loss in the United States—1979. Pediatrics 1981; 67:924-5.
9. Connolly BP, McNamara JA, Sharma S, Regillo CD, Tasman W. A comparison of laser photocoagulation with trans-scleral cryotherapy in the treatment of threshold retinopathy of prematurity. Ophthalmology 1998; 105:1628-31.
10. Gole GA. Animal models of retinopathy of prematurity. In: Silverman WA, Flynn JT, editors. Retinopathy of prematurity. Boston: Blackwell Scientific Publications; 1985. p. 53-95.
11. McLeod DS, D'Anna SA, Lutty GA. Clinical and histopathologic features of canine oxygen-induced proliferative retinopathy. Invest Ophthalmol Vis Sci 1998; 39:1918-32.
12. Nguyen T, Sherratt PJ, Pickett CB. Regulatory mechanisms controlling gene expression mediated by the antioxidant response element. Annu Rev Pharmacol Toxicol 2003; 43:233-60.
13. Owuor ED, Kong AN. Antioxidants and oxidants regulated signal transduction pathways. Biochem Pharmacol 2002; 64:765-70. Erratum in: Biochem Pharmacol 2002; 64:1547.
14. Prochaska HJ, De Long MJ, Talalay P. On the mechanisms of induction of cancer-protective enzymes: a unifying proposal. Proc Natl Acad Sci U S A 1985; 82:8232-6.
15. Friling RS, Bergelson S, Daniel V. Two adjacent AP-1-like binding sites form the electrophile-responsive element of the murine glutathione S-transferase Ya subunit gene. Proc Natl Acad Sci U S A 1992; 89:668-72.
16. Wasserman WW, Fahl WE. Functional antioxidant responsive elements. Proc Natl Acad Sci U S A 1997; 94:5361-6.
17. Dinkova-Kostova AT, Holtzclaw WD, Cole RN, Itoh K, Wakabayashi N, Katoh Y, Yamamoto M, Talalay P. Direct evidence that sulfhydryl groups of Keap1 are the sensors regulating induction of phase 2 enzymes that protect against carcinogens and oxidants. Proc Natl Acad Sci U S A 2002; 99:11908-13.
18. Day RM, Suzuki YJ, Fanburg BL. Regulation of glutathione by oxidative stress in bovine pulmonary artery endothelial cells. Antioxid Redox Signal 2003; 5:699-704.
19. Jaiswal AK. Regulation of genes encoding NAD(P)H:quinone oxidoreductases. Free Radic Biol Med 2000; 29:254-62.
20. Zhu M, Chapman WG, Oberley MJ, Wasserman WW, Fahl WE. Polymorphic electrophile response elements in the mouse glutathione S-transferase GSTa1 gene that confer increased induction. Cancer Lett 2001; 164:113-8.
21. Zhu M, Fahl WE. Development of a green fluorescent protein microplate assay for the screening of chemopreventive agents. Anal Biochem 2000; 287:210-7.
22. Zhu M, Fahl WE. Functional characterization of transcription regulators that interact with the electrophile response element. Biochem Biophys Res Commun 2001; 289:212-9.
23. Tomanin R, Scarpa M. Why do we need new gene therapy viral vectors? Characteristics, limitations and future perspectives of viral vector transduction. Curr Gene Ther 2004; 4:357-72.
24. Auricchio A, Kobinger G, Anand V, Hildinger M, O'Connor E, Maguire AM, Wilson JM, Bennett J. Exchange of surface proteins impacts on viral vector cellular specificity and transduction characteristics: the retina as a model. Hum Mol Genet 2001; 10:3075-81.
25. Ahrens ET, Feili-Hariri M, Xu H, Genove G, Morel PA. Receptor-mediated endocytosis of iron-oxide particles provides efficient labeling of dendritic cells for in vivo MR imaging. Magn Reson Med 2003; 49:1006-13.
26. Prow TW, Kotov NA, Lvov YM, Rijnbrand R, Leary JF. Nanoparticles, molecular biosensors, and multispectral confocal microscopy. J Mol Histol 2004; 35:555-64.
27. Lutty GA, Mathews MK, Merges C, McLeod DS. Adenosine stimulates canine retinal microvascular endothelial cell migration and tube formation. Curr Eye Res 1998; 17:594-607.
28. Selden SC 3rd, Schwartz SM. Cytochalasin B inhibition of endothelial proliferation at wound edges in vitro. J Cell Biol 1979; 81:348-54.
29. Mallory FB, Wright JH. Pathological technique: a practical manual for workers in pathological histology including directions for the performance of autopsies and for microphotography. Philadelphia: W. B. Saunders Company; 1938.
30. Shaner NC, Campbell RE, Steinbach PA, Giepmans BN, Palmer AE, Tsien RY. Improved monomeric red, orange and yellow fluorescent proteins derived from Discosoma sp. red fluorescent protein. Nat Biotechnol 2004; 22:1567-72.

The print version of this article was created on 26 May 2006. This reflects all typographical corrections and errata to the article through that date. Details of any changes may be found in the online version of the article.